

# Resonant optical electron transfer in one-dimensional multiwell structures

A V Tsukanov

Institute of Physics and Technology, Russian Academy of Sciences, Nakhimovsky pr. 34, Moscow 117218, Russia

E-mail: [tsukanov@ftian.ru](mailto:tsukanov@ftian.ru)

**Abstract.** We consider coherent single-electron dynamics in the one-dimensional nanostructure under resonant electromagnetic pulse. The structure is composed of two deep quantum wells positioned at the edges of structure and separated by a sequence of shallow internal wells. We show that complete electron transfer between the states localized in the edge wells through one of excited delocalized states can take place at discrete set of times provided that the pulse frequency matches one of resonant transition frequencies. The transfer time varies from several tens to several hundreds of picoseconds and depends on the structure and pulse parameters. The results obtained in this paper can be applied to the developments of the quantum networks used in quantum communications and/or quantum information processing.

PACS numbers: 03.67.Lx, 73.23.-b, 78.67.-n

Submitted to: *J. Phys. C: Solid State Phys.*

## 1. Introduction

The implementation of reliable connection between remote parts of quantum register remains one of the serious challenges on the way of realization of scalable quantum computations. One possible solution of this problem is to encode quantum information into the spin or charge state of single probe electron that can next be transferred from one qubit to another qubit with the help of an auxiliary quantum circuit. In the theoretical schemes of solid-state quantum information processing, such quantum networks based on regular arrays of specific quantum nodes (semiconductor quantum dots [1], quantum wells [2], quantum wires [3], donor atoms [4]), exploiting voltage-controlled tunneling for coherent electron transport, were recently proposed. The transfer protocols developed in the most of those works employ the stimulated adiabatic passage techniques adopted from the quantum optics. These methods were shown to be quite promising due to their robustness against unwanted transitions from the transport state. The electron transfer time depends on the distance between the sender and target nodes as well as on the voltage pulse design. In Ref. [3] it was reported on the possibility of complete electron transfer between two electrostatically defined quantum dots connected through the 600 nm long quantum wire. The calculated transfer time  $\tau \sim 50$  ps is short enough to allow coherent manipulations with the nonlocal charge electronic state. However, since the voltage driving schemes are very sensitive to imperfections in the time delays and in the shapes of voltage pulses, the requirements on the pulse engineering remain severe. This makes the realization of such transfer protocols to be difficult experimental task. Other strategies of selective electron transfer utilize the strong and rapid electromagnetic modulation of the potential relief of nanostructures [5, 6]. They rely upon the fact that the tunneling rate between neighboring nodes in the structure can be efficiently controlled by the field strength variation. At the same time, the strong fields acting on the auxiliary network will disturb the qubits in uncontrollable manner that may create insurmountable obstacle on the route of scalable quantum computer's building.

In this paper, we propose an alternative mechanism for the selective electron transfer between two edge identical quantum wells of the quasi-one-dimensional multiwell nanostructure, where internal wells form the body of the transport circuit. The probe electron, occupying initially the ground state of one of the edge wells, can be brought into interaction with the nearest qubit. Thus, the probe electron becomes entangled with this qubit, and its spin or charge state is conditioned by the qubit state. Being transported between two edge wells, the electron carries the information about the state of a given qubit onto the qubit attached to another edge well. Unlike conventional approaches involving correlated voltage gate switches to operate on electron charge state, we make use of  $\Lambda$  - type resonant optical excitation scheme proposed earlier to drive the single-qubit evolution in various double-well quantum systems [7] - [21]. At most two resonant terahertz pulses are required in this case, and very accurate population transfer can be attained in times of order of several tens of picoseconds and for the pulses of much more moderate strengths than in the strategies mentioned above. Here

we study a way how to choose the pulse and structure parameters in order to optimize the efficiency of addressed probe electron transfer. We analyze the transfer probabilities at different choices of the pulse strengths and frequencies as well as for different numbers of quantum wells forming the structure. Although the numerical results are obtained for an effective one-dimensional structure, the algorithm of the structure and pulse engineering developed here can be adopted for realistic solid-state nanostructures.

The paper is organized as follows. In Sec. II the parameters of individual quantum wells are selected in a way to form the reliable single-electron transport channel in the nanostructure composed of those wells. The energy spectrum and optical properties of multiwell nanostructure are considered in Section III. Section IV contains numerical data of the dynamical simulations. We conclude our study by Section V.

## 2. Single-well parameter choice

We begin with the description of the model of nanostructure employed in this work. The nanostructure is composed of  $N$  quantum wells (QWs) placed in series and separated by finite barriers. Two edge QWs with indices  $i = 1$  and  $i = N$  are deeper than the internal QWs. The energy spectrum of an electron confined in the structure is presented by two ground states (each of them being localized in corresponding edge QW) and  $N$  excited eigenstates delocalized over the structure. The latter result from the hybridization of the states of individual QWs due to the tunneling process. The localized states are supposed to be isolated from each other, i. e., the electron tunneling between them is negligibly small. If the electron occupies one of those states, it can stay there for extremely long time. The excited states of the nanostructure are approximately expressed by linear combinations of the states of isolated QWs [1]. Provided that the nanostructure is symmetric, the wave functions of the hybridized states have even or odd parity relative to the center of nanostructure. The degree of hybridization depends on the heights and the widths of the potential barriers separating neighboring QWs as well as on the differences in the corresponding eigenenergies of isolated QWs.

At the initial step, we choose the parameters of individual QWs. Several circumstances should be taken into account here. First, the ground states of the edge QWs are supposed to be strongly localized whereas the excited states of those wells must be close to the top of the potential barrier in order to form the reliable transport channel (through their hybridization with the states of neighboring internal QWs). Second, the matrix elements of optical dipole transitions (ODTs) between the localized and excited states of each edge QW have to be large enough to allow rapid optical excitation/deexcitation of an electron. It is known that the value of the ODT matrix element  $|d_{0,k}| = |\langle 0|ex|k\rangle|$  ( $e$  is the electron charge,  $x$  is the coordinate) between the ground state  $|0\rangle$  and an arbitrary excited state  $|k\rangle$  of a single QW goes down quickly with the quantum number  $k$  of the excited state. For a square QW with infinite walls it depends on the excited state number  $k$  as  $|d_{0,k}| \sim (k+1)/[k^2(k+2)^2]$ , where  $k$  is odd because of the selection rule. It means that each edge QW should be fabricated as a deep

narrow well containing only two bound electron states with  $k = 0$  and  $k = 1$ . Further, since the tunnel coupling between edge QWs is mediated by an array of identical internal QWs, to implement electronic transfer over longer distances, one has to utilize wider QWs and to increase the QW number  $N$ . From the other hand, it is desirable that each internal QW contain only one bound state. As a result, in order to meet above conditions the internal QWs should be designed as wide shallow wells.

Instead of commonly used square potential shape, we consider here a less-studied power-exponential (PE) form for QW potentials [22]:

$$U(x) = U_0 \exp \left[ - \left( \frac{x - x_0}{a_0} \right)^{2p} \right], \quad (1)$$

where  $U_0$  is the depth of potential well,  $a_0$  is the radius of potential, which determines the QW size,  $x_0$  is the coordinate of the center of potential, and parameter  $p$  defines the smoothness of QW boundaries. This kind of electron confinement is found to be a good approximation for the electrostatically-gated quantum dots in two- and three-dimensional cases [22]. Wide class of potentials can be modelled within this framework; in particular, a square QW potential is obtained from Eq. (1) if one sets  $p \gg 1$ . Note, that PE potentials are smooth functions of coordinate that considerably simplifies the numerical treatment of the eigenvalue problem.

The one-dimensional Schrödinger equation for a single electron moving in the potential  $U(x)$ ,

$$- \frac{\hbar^2}{2m^*} \frac{\partial^2}{\partial x^2} \Psi(x) + U(x) \Psi(x) = E \Psi(x), \quad (2)$$

is solved with the help of the finite-difference second-order scheme [23]. This procedure is equivalent to the solution of a system of uniform algebraic equations expressed by five-diagonal sparse matrix and, consequently, to finding the eigenvalues and eigenvectors of that matrix. The accuracy of the method is very high, and the finite-difference schemes of higher orders are generally excessive for treating the one-dimensional problems. The results of calculations are given in effective atomic (or donor) units - i. e., 1 a.u. =  $Ry^* = m^* Ry / m_e \varepsilon^2$  for the energy and 1 a.u. =  $a_B^* = m_e \varepsilon a_B / m^*$  for the length, where  $Ry$  is the Rydberg energy,  $a_B$  is the Bohr radius,  $m_e$  is the free electron mass,  $m^*$  is the effective electron mass, and  $\varepsilon$  is the dielectric constant. For GaAs one has  $Ry^* = 0.006$  eV and  $a_B^* = 10$  nm.

Here we demonstrate the solutions of Eq. (2) for a single QW with the PE potential of Eq. (1), where the potential radius  $a_0$  and the parameter  $p$  are fixed and the potential depth  $U_0$  is varied. We used the computational interval of length  $L=10$  with the number of grid points  $N_L=10000$  (at the boundaries of this interval the wave functions are set to zero). We take  $a_0 = 0.4$  for the edge QW,  $a_0 = 1$  for the internal QW, and  $p = 5$ ,  $x_0=0$  for both types of wells. The dependencies of low-lying part of the energy spectrum for the edge and internal QWs on  $U_0$  are presented in Figs. 1 (a) and 1 (b), respectively. We present the results for the values of  $U_0$  at which there are no more than two bound electron eigenstates with energies  $\varepsilon_0 < 0$  and  $\varepsilon_1 < 0$  in the QW. Other states, whose

energies  $\varepsilon_k$  are positive (hereafter - unbound or quasicontinuum states), belong to the spectrum of large square infinite potential well of the length  $L$ , modified by the QW in its central part. As the absolute value  $|U_0|$  of the QW depth decreases, the levels  $\varepsilon_0$  and  $\varepsilon_1$  shift to the barrier top. They interact with unbound states of the same symmetry giving rise to the anticrossing pattern. The presence of the symmetric QW potential in the center of computation interval amounts also to the energy splitting of states of the large well. We observe apparent doublet structures for the states with positive energies, which transform into the states of the large square well at vanishing  $U_0$ .

Figures 2 (a) and 2 (b) illustrate the dependencies of absolute values of ODT matrix elements  $|d_{0,k}|$  on the potential depth  $U_0$ . The values of the ODT matrix elements are given in atomic units  $|e|a_B^*$ . We see that the plot of  $|d_{0,1}|$  for the edge QW [Fig. 2 (a)] has a local maximum at  $U_0 \approx -24$ . At that point, other matrix elements of ODT are still small, and all excitations from the ground state of the edge QW to the quasicontinuum states remain inefficient. It is thus reasonable to take  $U_0 \approx -24$  for the edge QW. As the QW becomes shallower, one observes a sharp increase of the ODT matrix elements, which approach the values of the ODT matrix elements  $d_{0,k}^{(L)}$  of the large square well. The latter are much greater than the matrix elements of ODT between the bound states of deep QW; the values for both types of matrix elements relate each other as the corresponding effective potential lengths, namely,  $|d_{0,k}^{(L)}/d_{0,k}| \sim L/a_0$ , where  $L/a_0 \gg 1$ . At very large potential depths the matrix element  $d_{0,1}$  becomes close to the value  $d_{0,1}^{(0)} = 16el_0/9\pi^2$  for an infinite square well, where  $l_0 = 2a_0$  is the well width, and for  $a_0=0.4$  one has  $d_{0,1}^{(0)} = 0.14$ . In contrast to the edge QW, all of the ODT matrix elements of internal QWs should be selected as small as possible in order to minimize unwanted excitations of electron from bound state to the quasicontinuum states. As it is seen in Fig. 2 (b), the plot of  $|d_{0,1}|$  demonstrates a pronounced increase for  $U_0 \geq -2.5$ . Hence we choose  $-3 \leq U_0 \leq -2.5$  for the internal QW so that the first excited state is outside the QW but the values of the ODT matrix elements are still minor.

Making our choice of the value of  $U_0$  for edge QWs [Fig. 1 (a)], we fix the electronic eigenenergies  $\varepsilon_0$  and  $\varepsilon_1$  of the edge QWs; then from the plot of the ground state energy  $\varepsilon_0$  of internal QW vs  $U_0$  [Fig. 1 (b)] we define the value of  $U_0$  at which the energy  $\varepsilon_0$  of internal QWs is approximately equal to the excited state energy  $\varepsilon_1$  of the edge QWs. The results of calculations presented below are obtained for the following set of the parameters:  $a_0 = 0.4$ ,  $U_0 = -23.83$  for the edge QWs and  $a_0 = 1$ ,  $U_0 = -2.5$  for the internal QWs. From Figs. 1 (a) and 1 (b) one may see that the energy  $\varepsilon_1$  of the edge QWs slightly differs from the energy  $\varepsilon_0$  of the internal QWs. This is done intentionally in order to make our model of nanostructure more realistic since in practice it is very difficult to attain the exact adjustment of the QW levels.

### 3. The nanostructure

The  $N$  QWs stacked in the way described above constitute the body of a one-dimensional linear nanostructure. The energy spectrum of the nanostructure depends on the

parameters of individual QWs [the QW potential depths  $U_0(i)$  and the QW radii  $a_0(i)$ ,  $i = 1 - N$ ] and on the widths of the barriers separating the wells. For simplicity, we suppose that all of the distances  $b(i)$ ,  $i = 1 - (N - 1)$ , between the centers of neighboring QWs (hereafter - interwell distances) are the same and equal to  $b$ . In this case, the potential of nanostructure is given by the expression

$$U(x) = \sum_{i=1}^N U_0(i) \exp \left\{ - \left[ \frac{x - (i - 1/2 - N/2) b}{a_0(i)} \right]^{2p} \right\}, \quad (3)$$

where the origin of coordinate is placed into the center of nanostructure. Now we seek the solution of Eq. (1) with the potential having the form of Eq. (3) with the values of the edge and internal QW parameters selected above and  $p=5$ . The parameters for the edge (internal) QW are supplied with index 0 (1):  $U_0(i) = U_{0(1)}$ ,  $a_0(i) = a_{0(1)}$  if  $i = 1, N$  ( $i \neq 1, N$ ).

In what follows, we shall be interested in eigenenergies of not only the states bound in the QW structure, but also of states lying higher than the potential barrier. The accurate calculation of the energies of those quasicontinuum states requires a quite large computational length  $L$  and a great number  $N_L$  of grid points. We have computed the eigenenergies  $\varepsilon_k$  in the range  $\varepsilon_0 \leq \varepsilon_k \leq |\varepsilon_0|$  for different QW numbers  $N$  (up to  $N = 20$ ) at several sets of  $L$  and  $N_L$ . It was found that for all those nanostructures the choice  $L = 500$  and  $N_L = 40000$  enables one to satisfactory simulate the quasicontinuum states in the pointed energy interval.

In this Section, we examine in detail the nanostructure composed of six QWs, see Fig. 3 (a). The plots of the excited state energies  $\varepsilon_k$  ( $k=2 - 7$ ) on the interwell distance  $b$  (actually, on the barrier width) are presented in Fig. 3 (b). As expected, the energies  $\varepsilon_k$  depend on  $b$  exponentially. At the same time, they deviate from the tight-binding (TB) predictions [1] and bring about an asymmetrical distribution of  $\varepsilon_k$  relative to the center of the energy subband. This is the peculiarity of a real system, where the energy of a hybridized state is to be a function of the closeness of this state to the barrier top. In fact, the overall correspondence between the spectrum of our structure and the spectrum of structure modelled within the TB approximation [1] is mainly determined by the effective tunneling rates between neighboring QWs. Usually, it is expected that the weaker the tunneling the better this correspondence. Therefore, for deeper wells and wider barriers the results of TB model will give more accurate description of the nanostructure. Besides, the small detuning in the energies of individual QWs affects, to some extent, the mechanism of the state hybridization. For a quite large  $b$  ( $b \geq 4.5$ ), it results in a dissociation of the six-fold energy subband into the two degenerate energy levels ( $\varepsilon_2$  and  $\varepsilon_3$ ), presented by the even and odd superpositions of excited states of isolated edge QWs, and the four-fold subband of weakly-hybridized states with  $\varepsilon_{k \neq 2,3}$  pertaining to the internal part of the nanostructure. As follows from our calculations, the variation of the distance  $b_0$  between the centers of the edge QWs and the neighboring internal QWs at some fixed distance  $b_1$  between the centers of two neighboring internal QWs does not change noticeably the properties of the excited subband. The wave

functions  $\Psi_k(x)$  of the bound states  $|k\rangle$  ( $k=0 - 7$ ) are shown in Fig. 4. Note, that the wave functions  $\Psi_0(x)$  and  $\Psi_1(x)$  forming the ground state subspace of the Hilbert space of multiwell nanostructure are taken as the functions each localized in corresponding edge QW. This representation given by the isolated edge QW orbitals is equivalent to the representation given by their symmetric and antisymmetric combinations provided that the corresponding eigenenergies  $\varepsilon_0$  and  $\varepsilon_1$  of the Hamiltonian are almost degenerate.

Other important quantities, the ODT matrix elements, are plotted in Figs. 5 (a) and 5 (b). Due to the inversion symmetry of our structure, we may calculate the values of the matrix elements for only one excitation arm of the  $\Lambda$  scheme, e. g., involving the ground state  $|0\rangle$ , localized in the left QW ( $i=1$ ), and the excited states  $|k\rangle$  ( $k=2 - 7$ ). The ODT matrix elements for another excitation arm with the ground state  $|1\rangle$  of the right QW ( $i=N$ ), are related to them by the formula  $d_{1,k} = (-1)^k d_{0,k}$ . In the range of the interwell distances  $b$  around  $b=3$ , the values of matrix elements  $|d_{0,k}|$  for pairs of the states (doublets)  $\{|2\rangle, |7\rangle\}$ ,  $\{|3\rangle, |6\rangle\}$ , and  $\{|4\rangle, |5\rangle\}$  remain close to the corresponding values calculated in the TB model (denoted by horizontal dotted lines). As in the case of the energies, both data types do not coincide. This discrepancy can be explained in the following way. The TB wave functions of hybridized states are constructed from the isolated QW wave functions multiplied by the weight coefficients that depend on both the state number  $k$  and the QW index  $i$  [1]. Consequently, the ODT matrix element between the ground state  $|0\rangle$  and the hybridized state  $|k\rangle$  is simply the single-well matrix element  $d_{0,1}$  [Fig. 2 (a)] multiplied by the weight coefficient for the state  $|k\rangle$  in the edge QW ( $i=1, N$ ). For two quantum states of a given doublet, those coefficients are the same in one of the edge QWs and differ by the sign in another one. Hence, the moduli of the ODT matrix elements  $|d_{0(1),k}|$  for doublet states turn out to be equal to each other and do not depend on  $b$  under the TB approximation. However, we observe in Fig. 4 that the wave functions of doublet states have close but still different amplitudes in the edge QW regions. As a result, the matrix elements of ODT are different for the two doublet states. It means also that the wave functions of highly-delocalized states of the realistic nanostructure cannot be satisfactory approximated by the linear combinations of the wave functions of isolated QWs.

If the QWs are substantially remote from each other ( $b \geq 4.5$ ), the curves for  $|d_{0,2}|$  and  $|d_{0,3}|$  demonstrate asymptotical convergence to a common non-zero value whereas the others decay slowly to zero. Such a behavior of the ODT matrix elements indicates on the collapse of tunneling between the edge QWs and the internal part of nanostructure. Since the states  $|2\rangle$  and  $|3\rangle$  evolve with  $b$  into even and odd superpositions of excited states of the isolated edge QWs, the linear combination  $(|d_{0,2}| + |d_{0,3}|)/\sqrt{2}$  tends to the value of  $|d_{0,1}|$  for isolated edge QW. Note, that all of  $|d_{0,k}|$ , involving the quasicontinuum states  $|k\rangle$  ( $k > 7$ ), are very small in comparison with the values of matrix elements for ODTs between the bound states. [Several matrix elements for the transitions from the ground state into the quasicontinuum states are shown as thin black curves at the bottom of Fig. 5 (a)]. The explanation of this fact is rather simple. In general, the one-dimensional wave function of a localized electron may be presented

in a form  $\Psi_k(x) = \tilde{\Psi}_k(x)/\sqrt{l_k}$ , where  $k$  is the quantum number of the electron state,  $l_k$  is the characteristic length of electron spreading in this state, and  $\tilde{\Psi}_k(x)$  is the dimensionless function which amplitude is of order of unity. The ODT matrix element between the states  $|0\rangle$  and  $|k\rangle$  can thus be written as  $d_{0,k} = C_{0,k}el_0^2/\sqrt{l_0l_k}$ , where  $|C_{0,k}| \leq 1$ . Substituting here  $l_0 = l_k = a_0$ , we see that corresponding matrix element of the ODT, involving two bound states  $|0\rangle$  and  $|k\rangle$ , is of the order of  $ea_0$ . If, however, one sets  $l_0 = a_0$  and  $l_k = L$ , the estimation  $|d_{0,k}| \sim ea_0\sqrt{a_0/L} \ll ea_0$  is obtained. Both results are consistent with the numerical data presented in Fig. 5 (a).

Considering the next type of the matrix elements, we deal with the transitions between the states that constitute one subband. In Fig. 5 (b), we show the data illustrating the dependencies of such intrasubband ODT matrix elements on interwell distance  $b$  for the subbands  $\{|0\rangle, |1\rangle\}$  and  $\{|2\rangle - |7\rangle\}$ . In contrast to the intersubband ODT matrix elements  $d_{0,k}$  ( $k = 2 - 7$ ) that vary smoothly with  $b$ , the intrasubband matrix elements are approximately linear functions of the interwell distance. We observe also a strong increase in the values of the intrasubband ODT matrix elements in comparison with the intersubband ones. Besides, the intrasubband ODT matrix elements between neighboring states are significantly larger than those between non-neighboring states, pictured as thin black curves in Fig. 5 (b). According to the TB model, all intrasubband matrix elements are expressed by linear combinations of the diagonal single-well matrix elements. The latter describe the shifts of the energy levels of isolated QWs in an electric field. Their difference has a clear analogy in the classical physics: it is just the energy acquired by an electron transported between the QW centers in the electric field of unit strength. In the case of the diagonal matrix element for the localized state  $|0\rangle$ , the "classical" formula  $|d_{0,0}| = b(N - 1)/2$  perfectly reproduces the plot for  $|d_{0,0}|$  vs  $b$  found in the essentially quantum treatment of the problem. With that, as  $b$  increases, the plots of matrix elements for excited subband substantially deviate from the linear form. For example, the matrix element  $d_{2,3}$  initially separates from the others and then approaches  $d_{0,0}$  at  $b \geq 4.5$ . Again, it is because of the reorganization in the structure of hybridized states due to the tunneling collapse. Thus, the intrasubband ODT matrix elements not only account of the effects associated with the charge displacement in the external field, but also reflect the peculiarities of electronic density distribution in given quantum states.

The eigenenergies  $\varepsilon_n$  and matrix elements  $d_{m,n}$  of ODT calculated above will be used in the next Section in numerical study of the dynamical problem.

#### 4. Dynamics

We have mentioned in Introduction that there exist several ways of how to transport an electron from one QW to another in a semiconductor nanostructure. The aim of the present paper is to clarify some new aspects of resonant optical excitations in the effective  $\Lambda$  system formed in the spatially extended multiwell structure by a pair of ground states and a set of delocalized states. In the work [7], the symmetric three-level scheme was



employed to describe the resonant electron dynamics in the double-dot structure. It was shown that the square harmonic laser pulse of strength  $E(t) = E_0 \cos(\omega t)$  and duration  $T$  can produce complete population transfer between two spatially remote ground states  $|0\rangle$  and  $|1\rangle$  of the nanostructure if the pulse frequency  $\omega$  is tuned exactly to the resonance with the transitions  $\{|0\rangle, |1\rangle\} \rightleftharpoons |r\rangle$  connecting the ground state subspace and some excited (transport) state  $|r\rangle$  (other excited states are ignored). The accuracy of such a three-level approximation is very high provided that the following conditions imposed on the structure and pulse parameters are satisfied. (i) The transition frequency  $\omega$  is much larger than both the interlevel spacings  $|\Delta_{r,r\pm 1}| = |\varepsilon_r - \varepsilon_{r\pm 1}|$  and the coupling coefficient  $\lambda_{0,r} = E_0 d_{0,r}/2$ . It allows one to apply the so-called rotating wave approximation (RWA) under which an analytic solution of the dynamical problem is easily found. (ii) The coupling coefficient  $\lambda_{0,r}$  is rather small as compared with  $|\Delta_{r,r\pm 1}|$ . It guarantees the selectivity of resonant excitations, i. e., only the transport state  $|r\rangle$  is populated during the pulse action. (iii) The quantum dots (wells) are close enough to each other to neglect the diagonal coupling coefficients. It means that rapidly varying energy shifts do not modify appreciably the transition frequency  $\omega_{0(1),r}$  and thus do not violate the resonant conditions. The correction to the bare three-level scheme [7], accounting for a non-resonant excitation of the delocalized state nearest to the transport state, as well as the first-order correction to the RWA, were derived in Ref. [10].

Here we investigate the problem of the resonant field-structure interaction via fully-numerical treatment. We solve the one-electron non-stationary Schrödinger equation

$$i\hbar \frac{\partial}{\partial t} |\Psi(t)\rangle = H(t) |\Psi(t)\rangle \quad (4)$$

with the Hamiltonian

$$H(t) = H_0 - eE_0 x \cos(\omega t), \quad (5)$$

where  $H_0$  is the Hamiltonian of unperturbed nanostructure with the potential relief given by Eq. (3).

The state vector of the system may be presented in the form

$$|\Psi(t)\rangle = \sum_n c_n(t) e^{-i\varepsilon_n t/\hbar} |n\rangle, \quad (6)$$

where index  $n$  runs over the states belonging to the low-energy part of the nanostructure spectrum. Inserting Eqs. (5) and (6) into Eq. (4) and then multiplying Eq. (4) from the left side by  $\langle m|$  ( $m = 0, 1, 2, \dots$ ), we arrive at the set of linear differential equations for the probability amplitudes  $c_m(t)$ . It is convenient to rewrite this set in the following way:

$$i \frac{\partial c_m}{\partial t} = 2 \sum_n c_n \lambda_{m,n} \cos(\omega t) e^{-i\omega_{m,n} t} \quad (m = 0, 1, 2, \dots), \quad (7)$$

where  $\omega_{m,n} = \Delta_{m,n}/\hbar = (\varepsilon_n - \varepsilon_m)/\hbar$  is the transition frequency between the states  $|m\rangle$  and  $|n\rangle$ ,  $\lambda_{m,n} = \varepsilon_{field} d_{m,n}/2$  is the corresponding coupling coefficient,  $\varepsilon_{field} = ea_B^* E_0 / Ry^*$  is the field energy, and the time  $t$  is taken in units of  $\hbar / Ry^*$  (for GaAs 1 a.u.=0.11 ps).

For definiteness, assume that at  $t=0$  the electron is localized in the state  $|0\rangle$  in the left edge QW - i. e.,  $|\Psi(0)\rangle = |0\rangle$ , and hence the initial conditions for Eq. (7) read  $c_m(0) = \delta_{m,0}$ . Since our attention is concentrated on the possibility of complete population transfer between the ground states  $|0\rangle$  and  $|1\rangle$  of the multiwell nanostructure, here we restrict ourselves by analysis of the probability  $p_1(T) = |c_1(T)|^2$  to find the electron in the target state  $|1\rangle$  after the pulse is switched off. The numerical solutions of Eq. (7) have been obtained with the help of the non-stiff ode113 Matlab solver with relative accuracy  $\delta_{tol} = 10^{-6}$ . In all simulations we take the pulse frequency  $\omega$  to be equal to one of the nanostructure transition frequencies  $\omega_{0(1),r}$  ( $2 \leq r \leq 7$  for six-well structure). In this case, the single-electron dynamics is given by the resonant three-level Rabi oscillation picture. Typical plots of probabilities  $p_0(T)$  and  $p_1(T)$  of finding an electron in the states  $|0\rangle$  and  $|1\rangle$ , together with the total probability  $p_{tr}(T) = \sum_{k \neq 0,1} p_k(T)$  [ $p_k(T) = |c_k(T)|^2$ ] of electron to be out of ground-state subspace, versus the pulse duration  $T$ , are presented in Fig. 6 for  $r = 5$ ,  $N = 6$ .

The number of states, included into the simulations, was varied from 30 to 40. Apart from the bound states shown in Fig. 3 (a), we also took into account two groups of quasicontinuum states. The first group contains the states with energies  $0 < \varepsilon_k \ll |\varepsilon_0|$  lying in nearest neighborhood of the barrier top. It is expected that those states may affect, to some extent, the resonant dynamics in the bound state subspace through non-resonant excitations. The second group incorporates the states from the narrow energy interval located around the energy  $\varepsilon_r + \omega$ . Since those states are close to the two-photon resonance with the driving pulse, they could participate the electron evolution despite of small values of the corresponding ODT matrix elements. However, as one observes in Fig. 6, the resonant dynamics of an electron in the multilevel system is an essentially three-level dynamics. It is very close to that considered in Ref. [7] and is described by the formulae

$$p_0 = \cos^4(\Omega_R t), \quad p_1 = \sin^4(\Omega_R t), \quad p_r = \frac{1}{2} \sin^2(2\Omega_R t), \quad (8)$$

where  $\Omega_R = |\lambda_{0,r}|/\sqrt{2}$  is the Rabi frequency. It means that only the states  $|0\rangle$ ,  $|1\rangle$ , and  $|r\rangle$  play a decisive role in the electron dynamics, whereas the presence of other states is manifested in the weak modulations of ideal three-level plots. The participation of ladder resonant excitations involving quasicontinuum states as well as the processes beyond the RWA may be safely ignored due to the smallness of the parameters  $|\lambda_{r,k}|/|\lambda_{0,r}|$  ( $k > 7$ ) and  $|\lambda_{0,r}|/\omega$ . The transfer time  $T_0$  is thus defined from the condition  $\Omega_R T_n = \pi/2 + \pi n$  ( $n=0, 1, 2, \dots$ ) as the shortest pulse duration  $T_n$  at which the maximal population of target state  $|1\rangle$  is achieved - i. e.,  $T_0 = \pi/2\Omega_R$ . Note, that the definition of Rabi frequency  $\Omega_R$  is taken according to Refs. [7] and [10]; it differs by  $1/\sqrt{2}$  from that used in Ref. [11] for the description of resonant hydrogen molecular ion dynamics [cf. [11], Eq. (40)], since in that work the ground states of a molecular ion, as well as its excited states, were presented by even and odd linear combinations of the isolated atom states.

The most important question one has to answer is what a state from the excited subband should be used as the transport state  $|r\rangle$  in order to optimize the transfer

probability  $\max(p_1)$  and to reduce the transfer time  $T_0$ . According to the selectivity and high speed requirements, the values of  $|d_{0,r}|$  and  $|\Delta_{r,r\pm 1}|$  should be taken as large as possible. As it is clearly seen from both numerical data and analytical TB estimations, the states from the center of the excited energy subband (in the six-well structure the states  $|4\rangle$  and  $|5\rangle$ ) are characterized by the largest interlevel spacings and, at the same time, by the highest ODT matrix elements  $|d_{0,r}|$  than the states at the subband edges. We have performed the calculations of maximal transfer probabilities and transfer times at several fixed field energies  $\varepsilon_{field}$  (actually, the field strength) and for the different field frequencies  $\omega = \omega_{0,k}$  ( $k=2 - 7$ ). The results of calculations confirm our expectations, demonstrating that  $T_{0,k=4} < T_{0,k=5} < T_{0,k=3} < T_{0,k=6}$  in the whole range of  $\varepsilon_{field}$ . The pulse durations  $T_{0,k=2}$  and  $T_{0,k=7}$  corresponding to the electron transfer via edge excited subband states are significantly longer than others. Thus we come to the conclusion that the state closest to the center of excited subband is the best candidate for the transport state. If the QW number  $N$  is even, it will be one of states  $\{|N/2 + 1\rangle, |N/2 + 2\rangle\}$  of the central doublet, whereas for odd  $N$  this is the unpaired state  $|1 + (N + 1)/2\rangle$ .

The plots of the maximum values of  $p_1$ , see Fig. 7, demonstrate quasiperiodic behavior of the transfer probabilities on the field energy for each state of the pair  $\{|4\rangle, |5\rangle\}$  for  $N=6$ . We observe that the state  $|4\rangle$  displays better transport characteristics in comparison with the state  $|5\rangle$ . The maximum of the transfer probability  $\max(p_1) \approx 0.999$  for  $\omega = \omega_{0,4}$  is attained at quite large field energy  $\varepsilon_{field} = 0.083$ , thus allowing for rapid electron transfer (about 45 ps for the GaAs parameters). The transfer times  $T_0$  for both  $\omega = \omega_{0,4}$  and  $\omega = \omega_{0,5}$  cases are presented in Fig. 8. It is worth mentioning that the simple three-level expression for  $T_0$  (shown by the dashed curves) fits the numerical graphs very well.

In order to explain the dependencies of  $\max(p_1)$  on the field energy, we make a natural assumption that the oscillations in corresponding plots are caused by the presence of other excited states close to the transport state  $|r\rangle$ . In the work [10], we calculated the correction to ideal resonant three-level dynamics [Eq. (8)] taking into account the non-resonant occupation of the neighboring state  $|k\rangle$ . The corrected four-level formula for the population  $p_1$  of target state  $|1\rangle$  at  $T = T_0$  reads in current notations

$$p_1(T_0) \approx 1 - f_k, \quad f_k = (2\lambda_{0,k}/\Delta_{k,r})^2 \sin^2(\pi\Delta_{k,r}/2\sqrt{2}\lambda_{0,r}). \quad (9)$$

Note that this formula was derived via accurate solution of the four-level dynamical problem and contains more profound physics than those obtained by the simple adiabatic exclusion of the non-resonant levels.

The form of the set of Eqs. (7) assures that the non-resonant excitations of the delocalized nanostructure states  $|k\rangle$  ( $k \neq r$ ) occur independently up to the terms of higher orders in the parameters  $\lambda_{0,k}/\Delta_{k,r}$ , and the direct generalization of Eq. (9) to the multilevel  $\Lambda$  system results in the formula

$$\max(p_1) = p_1(T_0) \approx 1 - \sum_{k \neq r} f_k \quad (10)$$

(hereafter, the sum is over the bound states only). The dependencies of  $\max(p_1)$ ,

calculated through the Eq. (10), are visualized in Fig. 7 as the dashed curves. We see that for  $\omega = \omega_{0,4}$  the formula (10) is in a good agreement with the numerical data, while for  $\omega = \omega_{0,5}$  it gives overestimated values for local maxima of the transfer probability. What is the reason for such deviations? To our opinion, the main error originates from the neglecting in  $f_k = |c_k|^2$  [Eqs. (9) and (10)] the interference terms describing the correlation effects between the state  $|k\rangle$  and other excited states. Despite of the small values of these terms in comparison with non-correlated terms entering the formula (10), the correlated excitations may amount to some reduction of transfer probability. Besides, in the derivation of Eq. (9), the diagonal (intrasubband) coupling coefficients were ignored. These intrasubband terms of Eq. (7) oscillate at the field frequency  $\omega$  relative to the RWA frame and are usually discarded. However, since their values grow linearly with the interwell distance, they will affect the electron dynamics in extended structures, as  $\lambda_{m,n}$  become close to  $\omega$ .

We believe that the difference in the influence of one excited state on another excited state is explained by the difference in their ODT matrix elements  $|d_{0,k}|$ . For example, the value of  $|d_{0,4}|$  is larger than the value of  $|d_{0,5}|$ ; as a result, the population of the state  $|5\rangle$  is subjected to stronger modulations caused by the state  $|4\rangle$ , while the influence of the state  $|5\rangle$  on the the population of the state  $|4\rangle$  is less pronounced. It means that the state  $|4\rangle$  possesses better transport properties than the state  $|5\rangle$  and thus it should be selected as the transport state in the six-well nanostructure. The origin of oscillations of the transfer time  $T_0$  may be interpreted in a similar way. It should be noted that the first-order oscillating correction to  $T_0$  does not improve the accuracy of Eq. (10); this observation agrees with the arguments given above that several processes were neglected in derivation of Eq. (10). Nevertheless, the analytical curves yield rather accurate values of the local maxima positions in both cases. Therefore, Eq. (10) may be used at initial step for evaluation of the laser field strengths for which the probability of electron transfer is maximal. On the other hand, this formula enables us to study the dependence of  $\max(p_1)$  on the energy splittings  $\Delta_{k,r}$  that, in their turn, are the functions of the interwell distance  $b$  and the QW number  $N$ .

The important feature in the behavior of  $\max(p_1)$ , expressed by Eq. (10) and visualized in Fig. 9 for  $N = 6$ , is its band-like structure, where high transfer probability regions alternate with low transfer probability regions. We observe that  $\max(p_1)$  exhibits oscillations as  $b$  varies. Numerical data, plotted in Fig. 7 (a) for  $b = 3$ , lie at the vertical dashed line in Fig. 9. We have found that the value of  $\max(p_1)=0.999$  at  $\varepsilon_{field}=0.083$  (the point *A*) is likely to be the optimal one, since the closest maxima of  $\max(p_1)$  are lower. As predicted by the formula (10), if  $\varepsilon_{field}$  approaches 0.14, the dashed line crosses the region where the transfer probability substantially increases. At the point *B* ( $b=3$ ,  $\varepsilon_{field}=0.14$ ) the analytical value of  $\max(p_1) = 0.991$  correlates well with the numerical value of  $\max(p_1) = 0.988$ . It should be noted that, despite of the appreciable decrease in the transfer probability in comparison with the point *A*, the value of transfer time  $T_0 = 250$  for  $\varepsilon_{field} = 0.14$  is about half of  $T_0 = 420$  for  $\varepsilon_{field} = 0.083$ . We have also performed the calculations of  $\max(p_1)$  for the set of field and structure parameters chosen from the

high probability band containing the points  $C$  and  $D$  (see Fig. 9). Again, the numerical data are close to the analytical results, and  $\max(p_1)$  grows monotonically from 0.94 to 0.98, as we move from  $C$  to  $D$  along the dashed broken line, whereas the transfer time decreases from 419 to 252. Going beyond the point  $D$ , we arrive at the crossing region between this band and the vertical dashed line marking  $b = 3$ , that covers the field energy interval around  $\varepsilon_{field} = 0.2$  (not shown). For  $\varepsilon_{field} = 0.2$  we obtain  $\max(p_1) = 0.986$  that is smaller than the value computed at the point  $B$ , but the corresponding transfer time  $T_0 = 175$  appears to be very short. It means that if we are interested in fast electron transfer with moderate reliability, it is recommended to take  $\varepsilon_{field} = 0.2$  instead of  $\varepsilon_{field} = 0.083$ . At large values of the parameters  $\varepsilon_{field}$  and  $b$ , the probability of successful electron transfer becomes quite low (dark area in a right-up part of Fig. 9). This result is consistent with that obtained earlier (see Refs. [10] and [11]) and is explained in terms of the tunneling collapse.

At the final step, we have performed numerical simulations on the electron dynamics in the nanostructure composed of  $N$  QWs, where the QW number varies from  $N = 5$  to  $N = 20$ , and  $b = 3$ . If  $N$  is not large ( $5 \leq N \leq 12$ ), the dependencies of  $\max(p_1)$  on the field energy  $\varepsilon_{field}$  resemble those shown in Fig. 7 and demonstrate quasiregular oscillations with the amplitude increasing smoothly with  $N$ . For  $N \geq 17$ , the plots of  $\max(p_1)$  versus  $\varepsilon_{field}$  exhibit a "sawtooth" profile with sharp deeps and peaks. Again, we make use of Eq. (10) as the approximation for  $\max(p_1)$ , when the central state of the excited subband serves as the transport state. We find that the shapes of numerical and analytical curves of  $\max(p_1)$  deviate substantially from each other, if  $N$  approaches 20, whereas the correspondence between the values of peak positions remains surprisingly good. A general tendency is the shrinking of the region, where the values of  $\max(p_1)$  exceed 0.99. The last pronounced peak of  $\max(p_1)$  moves from  $\varepsilon_{field} = 0.2$  for  $N = 6$  to  $\varepsilon_{field} = 0.08$  for  $N = 20$ . We reveal, however, that the transfer times  $T_0$  taken at the peaks of  $\max(p_1)$  are very close to each other for different  $N$ . In Fig. 10 we present the dependencies of  $T_0$  on  $\varepsilon_{field}$  for  $N = 15, 16, 17$ , and 18. The points of interest, where  $0.99 \leq \max(p_1) \leq 0.999$ , are marked by open (filled) squares for odd (even)  $N$ . It is easy to see that each group of peaks, pertaining to different  $N$ , corresponds to a narrow range of  $T_0$  values. This observation enables us to make an important conclusion that the electron transfer time in multiwell nanostructure is not strictly defined by the number of QW in the structure, as it might be expected, but displays rather complex behavior conditioned by both the structure and field parameters. As the final remark, we note that the optimal points of the transfer probability lie in the middles of graph steps, where the analytic expression  $T_0 = \pi/|\lambda_{0,r}|\sqrt{2}$  yields very accurate values of the electron transfer time. Thus it is expected that this simple formula can be used to estimate  $T_0$  in the multiwell nanostructures regardless the QW number  $N$ .

## 5. Conclusions

In this paper, we have investigated theoretically the important and very actual problem of coherent single-electron transfer between two remote quantum wells in the semiconductor linear nanostructure. Apart from wide interest to the fundamental question addressing the possibility of reliable control over individual charge carrier dynamics in the solid-state low-dimensional structures, this study has a clear practical application - i. e., the organization of indirect connections in the ordered arrays of quantum bits.

For this purpose we make use of an auxiliary nanostructure containing a single electron in the quantized part of its conduction band. The resonant monochromatic laser pulse, applied to the structure, drives the electron evolution in such a way that, being initially localized in one quantum well, it comes onto another well at the end of the pulse. This process is influenced by many factors. In order to optimize the protocol - i. e., to attain high probability of electron transfer in short time, one should to choose carefully both structure and external field parameters. As we have found, the maximum electron transfer probability is a quasiperiodic function of the pulse strength and the interlevel spacings in the excited subband. The choice of one of excited states close to the subband center as the transport state is substantiated by an observation that this state possesses large ODT matrix element and is far enough from the others. It provides high transfer characteristics such as speed and selectivity.

Finally, it may be expected that the driving schemes relied upon the stimulated Raman adiabatic passage (STIRAP) [17, 24, 25] together with optimal control techniques [20] will enhance the efficiency of optically-induced single-electron transfer in the multiwell nanostructures.

## 6. References

- [1] Petrosyan D and Lambropoulos P 2006 *Optics Comm.* **264** 419
- [2] Cole J H, Greentree A D, Das Sarma S, and Hollenberg L C L 2008 arXiv:cond-mat/0802.2398
- [3] Bednarek S, Szafran B, Dudek R J, and Lis K 2008 *Phys. Rev. Lett.* **100** 126805
- [4] Skinner A J, Davenport M E, and Kane B E 2003 *Phys. Rev. Lett.* **90** 087901
- [5] Burdov V A and Solenov D S 2002 *Phys. Lett. A* **305** 427
- [6] Weiss C 2006 *Phys. Rev. B* **73** 054301
- [7] Openov L A 1999 *Phys. Rev. B* **60** 8798
- [8] Openov L A and Tsukanov A V 2004 *Pis'ma Zh. Eksp. Teor. Fiz.* **80** 572 [*JETP Lett.* **80** 503 ]
- [9] Tsukanov A V and Openov L A 2004 *Fiz. Tekh. Poluprovodn. (S. Peterburg)* **38** 94 [*Semiconductors* **38** 91]
- [10] Tsukanov A V 2006 *Phys. Rev. B* **73** 085308
- [11] Tsukanov A V 2007 *Phys. Rev. B* **76** 035328
- [12] Basharov A M and Dubovis S A 2005 *Opt. Spektrosk.* **99** 802 [*Opt. Spectrosc. (Russia)* **99** 770]
- [13] Amin M H S, Smirnov A Yu, and Maassen van den Brink A 2003 *Phys. Rev. B* **67** 100508(R)
- [14] Paspalakis E, Kis Z, Voutsinas E, and Terzis A F 2004 *Phys. Rev. B* **69** 155316
- [15] Kuan W-H, Tang C-S, and Chang C-H 2007 *Phys. Rev. B* **75** 155326
- [16] Brandes T, Renzoni F, and Blick R H 2001 *Phys. Rev. B* **64** 035319
- [17] Kis Z and Paspalakis E 2004 *Phys. Rev. B* **69** 024510

- [18] Førre M, Hansen J P, Popsueva V, and Dubois A 2006 *Phys. Rev. B* **74** 165304; Popsueva V, Førre M, Hansen J P, Kocbach L 2007 *J. Phys.: Condens. Matter* **19** 196204
- [19] Liao Y Y, Chuu D S, and Chen Y N 2007 *Phys. Rev. B* **75** 125325
- [20] Kosionis S G, Terzis A F, and Paspalakis E 2007 *Phys. Rev. B* **75** 193305
- [21] Räsänen E, Castro A, Werschnik J, Rubio A, and Gross E K U 2008 *Phys. Rev. B* **77** 085324
- [22] Ciurla M, Adamowski J, Szafran B, and Bednarek S 2002 *Physica E* **15** 261
- [23] Chelikowsky J R, Troullier N, Wu K, and Saad Y 1994 *Phys. Rev. B* **50** 11355
- [24] Bergmann K, Theuer H, and Shore B W 1998 *Rev. Mod. Phys.* **70** 1003
- [25] Vitanov N V and Stenholm S 1999 *Phys. Rev. A* **60** 3820

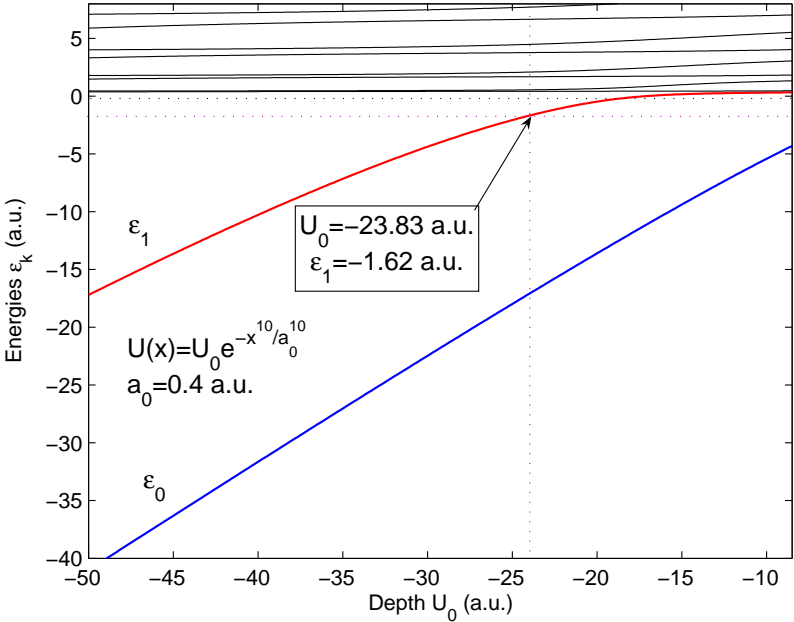


Fig. 1 (a)

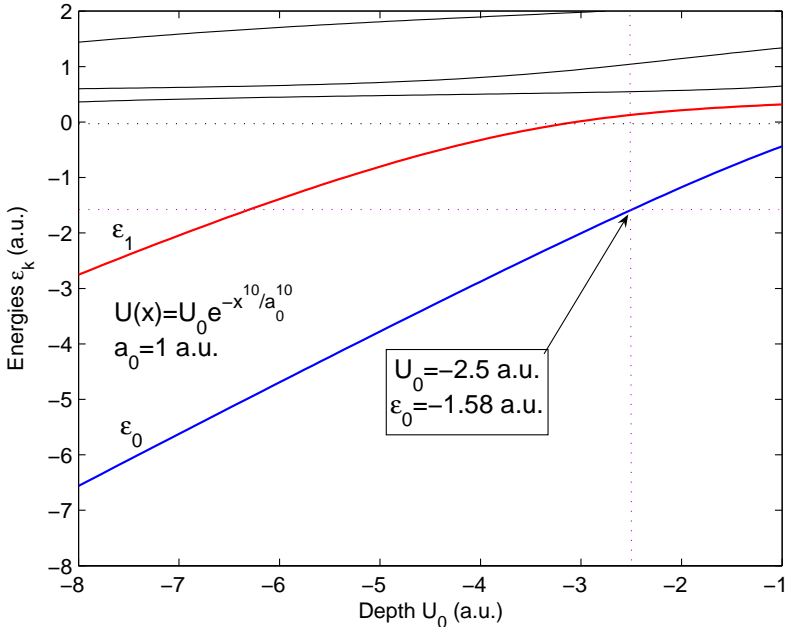


Fig. 1 (b)



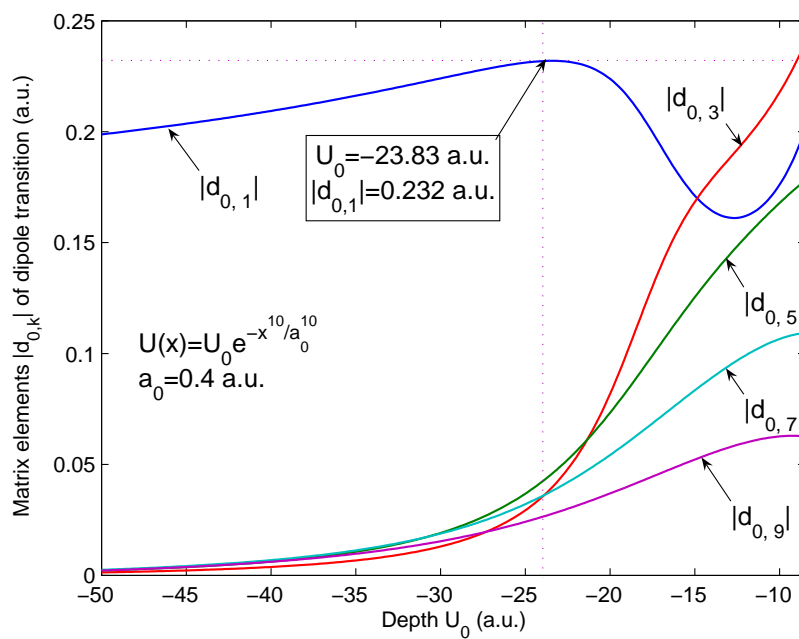


Fig. 2 (a)

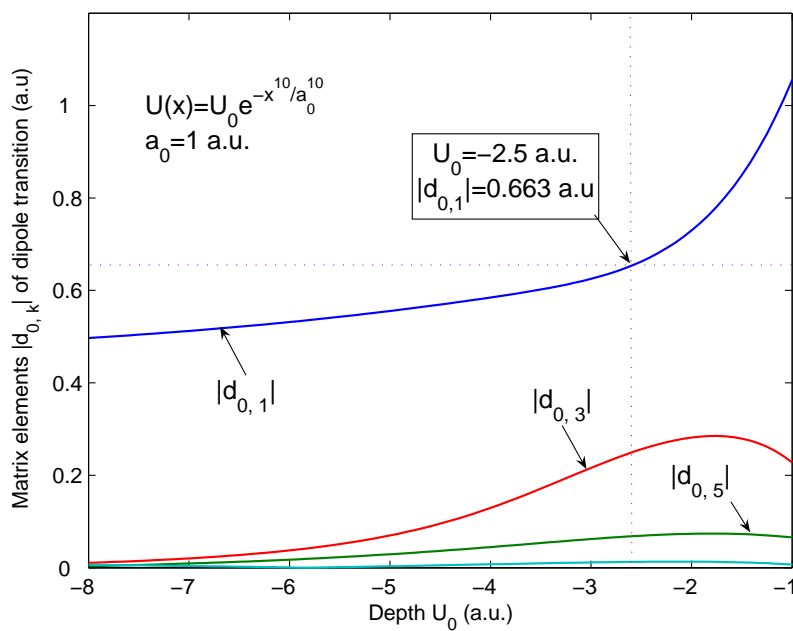


Fig. 2 (b)

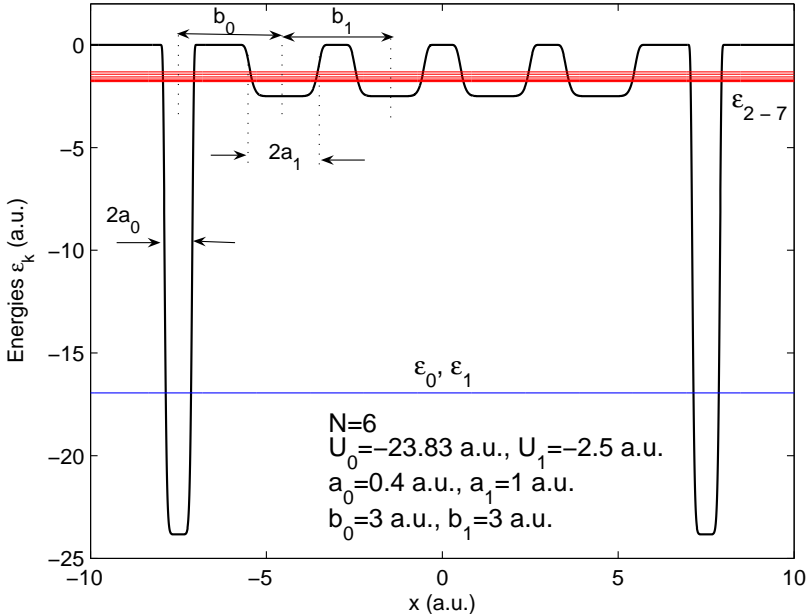


Fig. 3 (a)

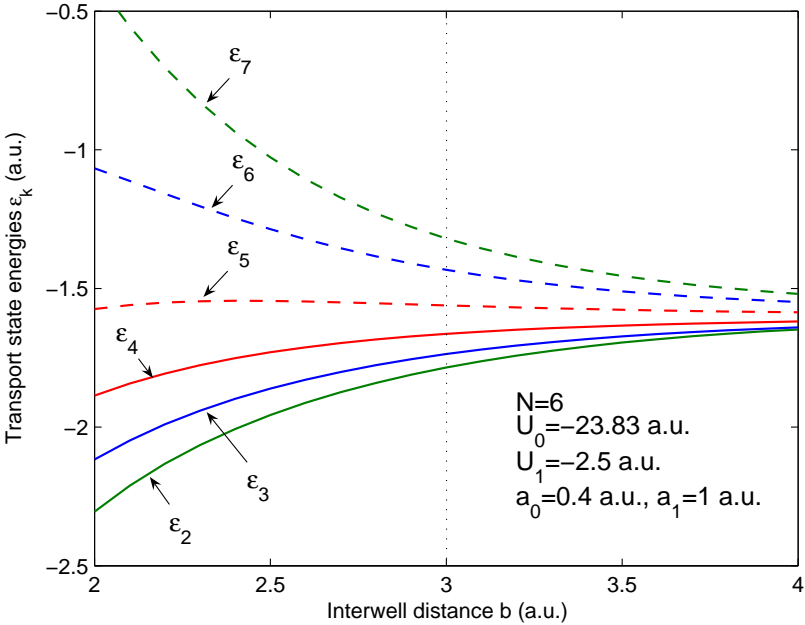


Fig. 3 (b)

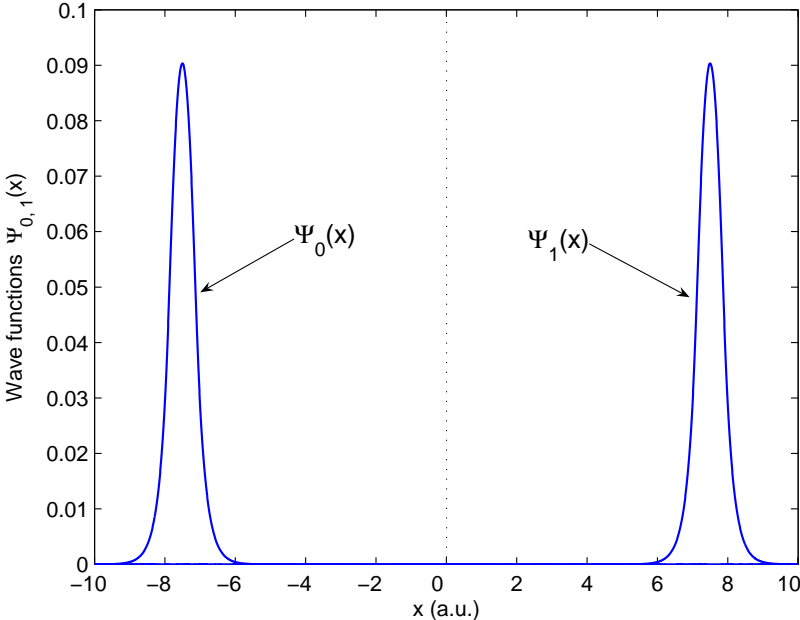


Fig. 4 (a)

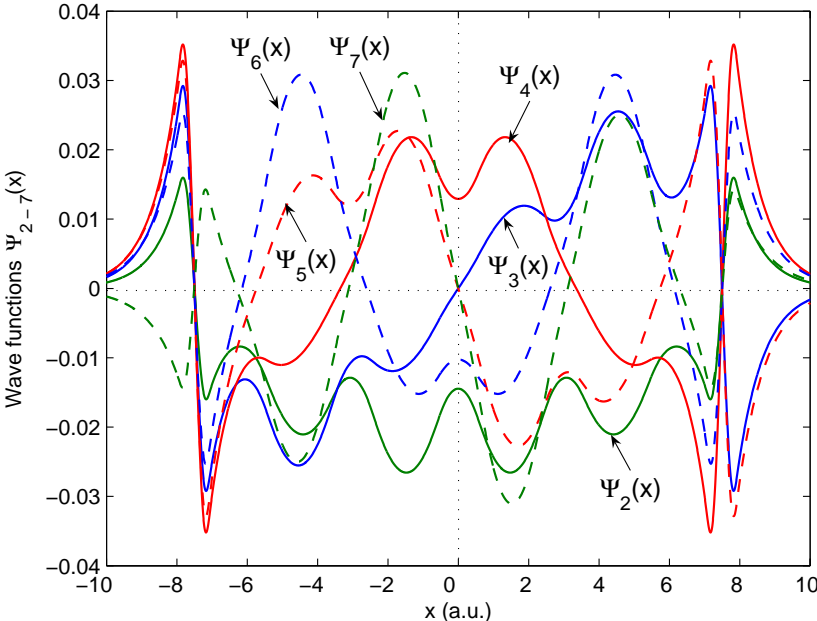


Fig. 4 (b)

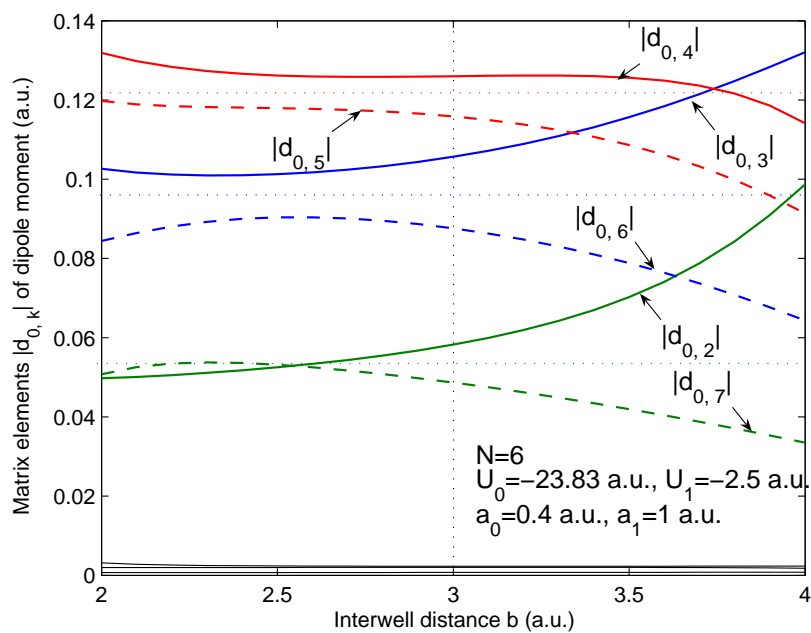


Fig. 5 (a)

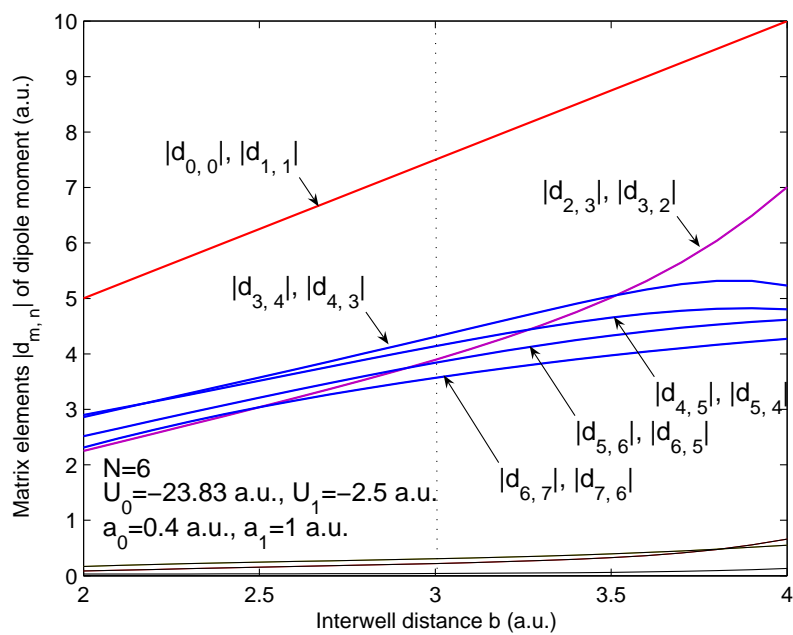


Fig. 5 (b)

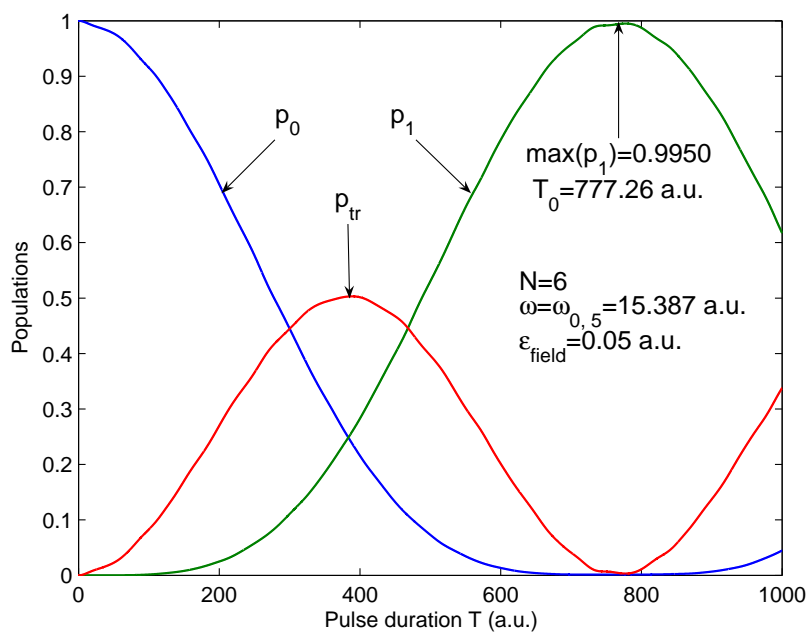


Fig. 6

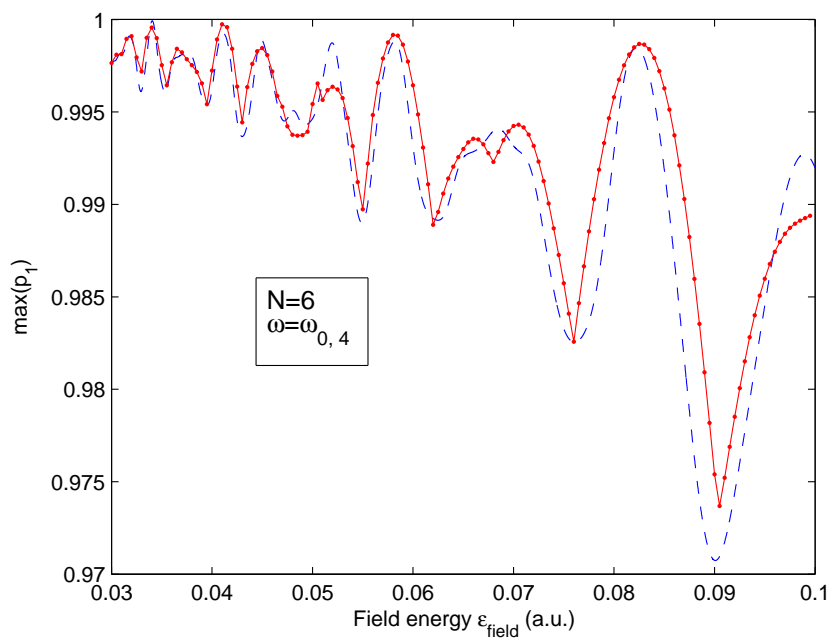


Fig. 7 (a)

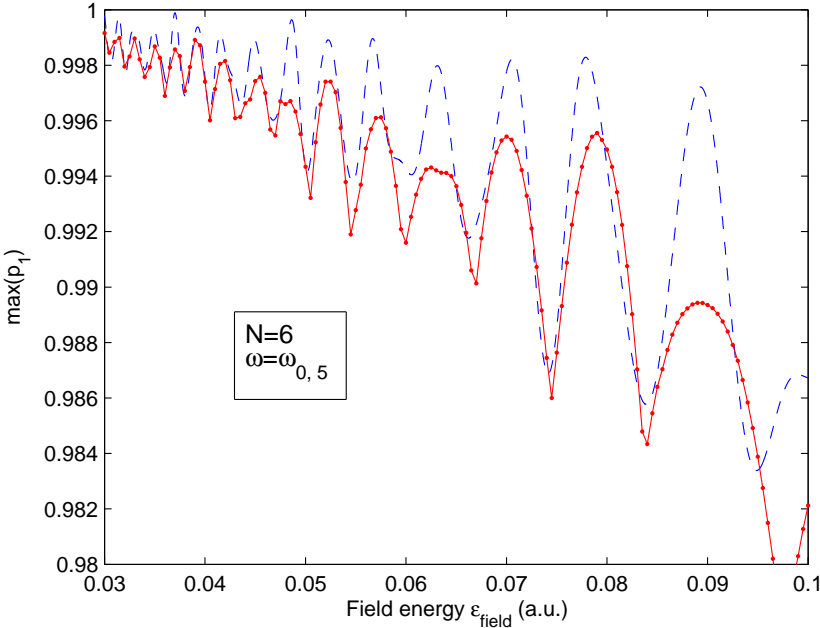


Fig. 7 (b)

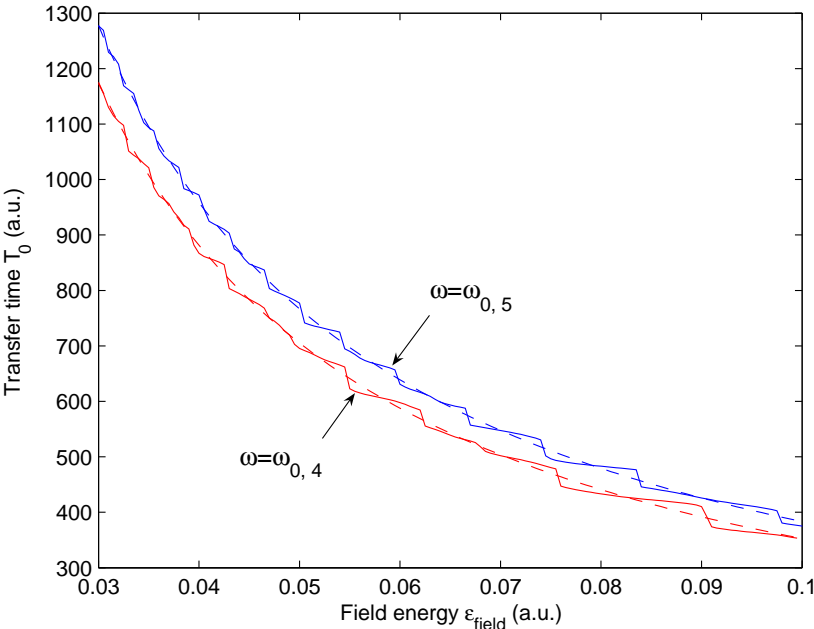


Fig. 8

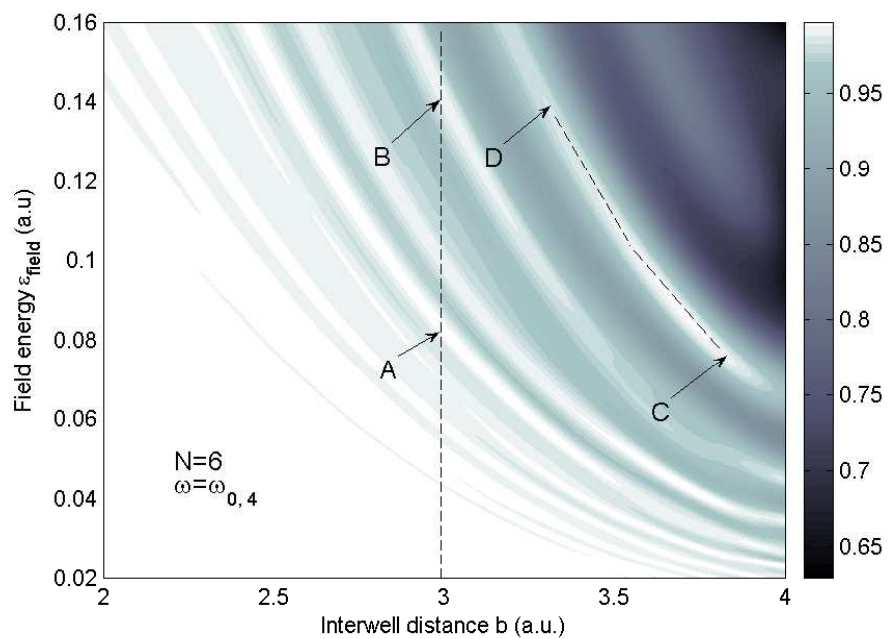


Fig. 9

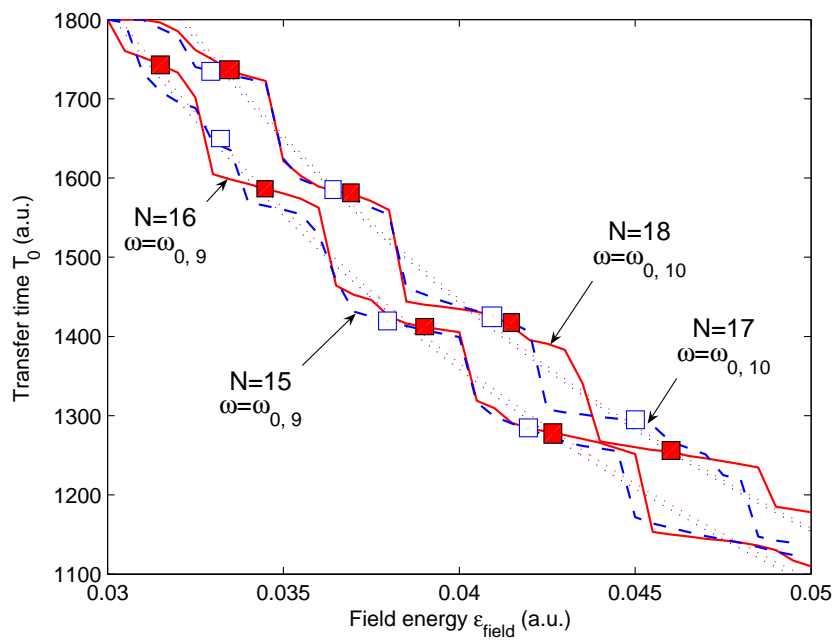


Fig. 10

## Figure captions

**Figure 1.** (color online). The dependencies of electronic eigenenergies  $\varepsilon_k$  of low-lying eigenstates of a single PE quantum well on the potential depth  $U_0$  for a) the edge quantum well and b) the internal quantum well. The well parameters used in further numerical calculations are shown in the insets.

**Figure 2.** (color online). The values  $|d_{0,k}|$  of matrix elements of optical dipole transitions, connecting the ground state  $|0\rangle$  and the low-lying excited states  $|k\rangle$  for a) the edge quantum well and b) the internal quantum well.

**Figure 3.** (color online). The six-well one-dimensional nanostructure placed in the central part of the large quantum well ( $L = 100$  a.u.). a) Potential profile  $U(x)$  of the structure in the case of  $b_0 = b_1 = 3$  a.u. and the energy levels  $\varepsilon_k$  from ground ( $k=0, 1$ ) and first-excited ( $k = 2 - 7$ ) subbands. b) The dependencies of the excited state energies  $\varepsilon_k$  ( $k = 2 - 7$ ) on the interwell distance  $b = b_0 = b_1$ . Vertical dotted line marks the value  $b = 3$  a.u. at which the most of numerical simulations are performed. Other parameters are given in the plot.

**Figure 4.** (color online). The plots of the electron wave functions for low-lying states of the six-well nanostructure (in arbitrary units) vs the coordinate  $x$  at  $b=3$  a.u. a) Ground-state wave functions  $\Psi_0(x)$  and  $\Psi_1(x)$ ; b) Excited-state wave functions  $\Psi_k(x)$ ,  $k = 2 - 7$ .

**Figure 5.** (color online). The absolute values of ODT matrix elements of the six-well nanostructure as the functions of interwell distance  $b$ . a) Intersubband matrix elements  $|d_{0,k}|$ . The horizontal dotted lines designate the values of  $|d_{0,k}|$  calculated in the TB approximation. b) Intracsubband matrix elements  $|d_{m,n}|$ .

**Figure 6.** (color online). The populations  $p_0$  and  $p_1$  of the ground states  $|0\rangle$  and  $|1\rangle$ , and the total population  $p_{tr}$  of excited states  $|k\rangle$ ,  $k \geq 2$ , vs the pulse duration  $T$ . The structure and pulse parameters as well as the value of the transfer probability  $\max(p_1)$  are shown on the plot.



**Figure 7.** (color online). The maximum transfer probability  $\max(p_1)$  of electron in the six-well nanostructure plotted as a function of the field energy  $\varepsilon_{field}$  for two choices of the transport state: a)  $r=4$  and b)  $r=5$ . The numerical solutions are presented by the solid curves (the calculated points are denoted by circles); the approximations of Eq. (10) are shown by the dashed curves.

**Figure 8.** (color online). The transfer time  $T_0$  between the ground states of the six-well structure vs the field energy  $\varepsilon_{field}$  for two choices of the transport state,  $r=4$  and  $r=5$ . The plots visualizing the approximation  $T_0 = \pi/|\lambda_{0,r}|\sqrt{2}$  are presented by dashed curves.

**Figure 9.** (color online). The transfer probability  $\max(p_1)$ , Eq. (10), as a function of both the interwell distance  $b$  and the field energy  $\varepsilon_{field}$ . The dashed lines denote the paths along which the numerical simulations were performed.

**Figure 10.** (color online). The transfer times  $T_0$  vs the field energy  $\varepsilon_{field}$  for the QW numbers  $N = 15, 17$  (blue dashed curves, open squares) and  $N = 16, 18$  (red solid curves, filled squares). The analytic data are shown by thin dotted curves.